Influence of Aluminum Doping on Ferrihydrite Nanoparticle Reactivity

Teresa L. Jentzsch and R. Lee Penn*

Department of Chemistry, University of Minnesota, Minneapolis, Minnesota 55455

Received: February 14, 2006; In Final Form: May 1, 2006

The composition of natural ferrihydrite varies considerably, especially in terms of aluminum and silicon substitution. This work examines the influence of aluminum content on the redox reactivity of ferrihydrite nanoparticles as determined by kinetic studies of the reductive dissolution of the particles by hydroquinone. Transition state theory applied to variable-temperature experiments is used to measure the activation enthalpy and entropy. The presence of small amounts of aluminum (0−2.1 mol % substitution) causes a decrease in $\Delta H^{\ddagger}$ and an increase in $\Delta S^{\ddagger}$, resulting in an overall increase in reactivity.

Introduction

Iron oxides are commonly found at and near the earth's surface as nanoparticles in the 3−10 nm size range and can be formed through a variety of mechanisms, including precipitation, redox, and weathering processes.[1,2] Because of their abundant presence, redox reactivity, and surface activity (e.g., adsorption affinity), iron oxide nanoparticles play important roles in the transformation and mobility of environmentally relevant species, including heavy metals, pollutants, and even naturally occurring chemical species. Arsenic, for example, has been shown to be transported through and subsequently released into groundwater by phase transformations and dissolution of iron oxide nanoparticles.[3,4] Finally, some bacteria couple the reduction of Fe(III) with the metabolism of organic materials, which can include anthropogenic contaminants, or simply use iron oxides as electron sinks during respiration.[5]

Ferrihydrite ($Fe_5HO_8{\cdot}4H_2O$)[1] is typically considered a metastable iron oxide that can act as a precursor to the more stable iron oxides such as goethite and hematite.[1,6] It forms as small (generally 4−6 nm), poorly crystalline particles and is classified according to the number of lines, usually two or six, observed in the X-ray powder diffraction pattern. Natural ferrihydrites are commonly found in spring- and groundwater[7] and as components of soils where water lies stagnant, such as drainage sites.[8] The high surface area and low crystallinity of these particles contribute to their enhanced reactivity relative to other iron oxides[9] and, therefore, their potential to influence environmental processes.

The soils and waters in which ferrihydrites often form are commonly rich in aluminum. Indeed, many environmental samples of iron oxides contain large amounts of aluminum impurity.[1,10] Studies have shown that this aluminum content may be as high as 32 mol % substitution.[1] The incorporation of a redox inactive species such as aluminum is expected to affect the chemical properties of iron oxide nanoparticles. Therefore, to better understand the behavior of natural iron oxides, the effects of cation substitution must be examined. Previously, researchers have studied the effects of varying amounts of aluminum on the reactivity of other environmentally relevant iron oxides such as goethite.[11,12] These studies showed that small amounts of aluminum appeared to enhance reactivity, while greater amounts of substitution inhibited reaction. To our knowledge, no studies have been performed on aluminum-substituted ferrihydrites. This paper specifically examines the abiotic reduction of well-characterized ferrihydrites with aluminum doping ranging from 0 to 2.1 mol %.

To quantitatively compare the reactivities of ferrihydrite samples with various amounts of aluminum doping, the rate of reductive dissolution of ferrihydrite by hydroquinone was monitored at several temperatures. Hydroquinone was selected as the reducing agent for its environmental relevance and the ease with which aqueous concentrations of this compound and its oxidation product can be characterized by analytical chemistry techniques.[13,14] Quinone functional groups are known to act as electron acceptors when bacteria reduce humic substances, which may subsequently reduce iron(III)-bearing minerals.[15] It is also believed that bacteria may secrete quinones to serve as electron shuttles during the reduction of insoluble metal oxides, including ferrihydrite.[16] Transition state theory was then applied to the resulting kinetic data in order to quantify the effect of aluminum substitution on chemical reactivity. Finally, extensive materials characterization was performed so as to ensure that the differences observed reflect the influence of aluminum doping as opposed to the influence of physical differences, such as particle size or morphology.

Experimental Methods

Synthesis of Al-Doped Ferrihydrites. Ferrihydrite nanoparticles were prepared using a method adapted from Burleson and Penn.[17] Four samples of ferrihydrite with various amounts of aluminum doping were precipitated from aqueous solutions of $Fe(NO_3)_3{\cdot}9H_2O$ and $Al(NO_3)_3{\cdot}9H_2O$ (ACS grade, Fisher). Solutions of the salts were prepared such that the total concentration of metal cations was 0.40 M; the percentage of aluminum ion present was between 0 and 30 mol %. To each solution, an equal volume of 0.48 M (for 0%, 5%, and 20% Al samples) or 0.64 M (for a 30% Al sample) $NaHCO_3$ (ACS grade, Mallinckrodt) was added dropwise, with stirring, over a period of 23 ± 0.3 min, resulting in an approximate final solution pH of 2.5. The deep-red suspension that resulted was heated by microwave for three 40 s intervals with intermediate shaking until boiling occurred and was then immediately placed into an ice bath. The suspension was dialyzed against purified water (Milli-Q) over a period of 4 days, with the water replaced

* penn@chem.umn.edu.

10.1021/jp060957+ CCC: $33.50
Published on Web 05/26/2006

nine times with a minimum of 3 h between each water change. After dialysis, the suspension was poured into shallow dishes to dry. The shiny, deep-red solid that resulted was ground into a fine reddish-brown powder and stored in a glass vial.

Materials Characterization. The materials were characterized using inductively coupled plasma mass spectrometry (ICP-MS), X-ray diffraction (XRD), and transmission electron microscopy (TEM).

ICP-MS samples were prepared by dissolving the solid particles in a solution of 4.8 M HCl and 3.2 M HNO_3, followed by dilution in 0.1 M HNO_3. The diluted solutions were analyzed for Fe, Al, As, and Na cation content using a ThermoElemental PQ ExCell quadrupole ICP-MS. Each sample was analyzed in duplicate, and concentrations were determined using a four-point calibration curve for each cation.

X-ray diffraction was performed using a PANalytical X'pert PRO MPD X-ray diffractometer equipped with an X'Celerator detector and cobalt source. Powdered samples were back-loaded into XRD sample holders to create flat surfaces. Data was collected over the range of 10−100° 2θ at a scan rate of 1°/min. The diffraction patterns were compared to the reference powder diffraction file (PDF) for 6-line ferrihydrite (PDF #29-0712) and the PDFs for the other iron oxides. Differential plots were determined by subtracting the XRD patterns for the 0% Al ferrihydrite from the Al-doped materials in order to assess changes in lattice parameters as a result of the aluminum doping.

Samples for transmission electron microscopy (TEM) were prepared by diluting a small amount of the suspended particles by ~1000 times using Milli-Q water, sonicating the diluted suspension, and placing one drop onto a 3 mm, 200 mesh holey carbon-coated copper grid (SPI). The samples were then allowed to air-dry. Images were collected using an FEI Tecnai T12 TEM operated at 120 kV. All images were collected using a charge-coupled device (CCD) camera and were analyzed using Gatan Digital Micrograph 3.3.1. The surface area of the samples was determined from length and width measurements of approximately 500 individual particles, which were modeled as ellipsoids. Using the standard equation for the volume of an ellipsoid and the equation for the surface area of a cigar-shaped ellipsoid, the average surface area per average volume for the particles was calculated. From the surface area per volume and the density of ferrihydrite (3.96 g/cm^3),[1] the specific surface area was calculated for each sample. TEM was used exclusively for surface area determinations, as previous BET measurements on ferrihydrites have demonstrated that such measurements are unreliable, at best, for these materials.[9]

Kinetic Reactions. Each reaction used 50 mg of solid sample, which was massed into a 60 mL amber glass vial (for heated reactions) or a 30 mL Nalgene bottle (for cooled reactions) and was placed in an anaerobic chamber (<100 ppm O_2). Following the addition of 5 mL of deoxygenated acetate buffer (40 mM, pH 3.75, acetic acid (Mellinckrodt) and sodium hydroxide (Titristar) in Milli-Q water), samples were sonicated, vortexed, and stirred overnight to further reduce aggregation of the particles. Nalgene bottles were wrapped in aluminum foil to block light since benzoquinone is known to photodegrade. Prior to reaction, an additional 19.5 mL of acetate buffer was added, and the samples were placed into an ice bath or a silicon oil bath heated to 30, 40, or 50 °C. After the temperature had equilibrated, 0.5 mL of 10 mM hydroquinone (Sigma), which was prepared using the deoxygenated acetate buffer, was added to initiate the reaction and bring the total suspension volume to 25 mL. At regular time intervals, 1 mL aliquots of the reaction mixture were quenched by filtration through 0.2 μm Acrodisc filters and into amber vials. The solutions were clear following filtration, indicating that the solid was removed from the reaction mixture. The filtered solutions were immediately analyzed using high-performance liquid chromatography (HPLC), as described below. The temperature was recorded at the beginning and end of each reaction to ensure that it had remained stable, and each reaction was performed in duplicate. Blanks were prepared in an identical manner, but omitting the solid ferrihydrite sample.

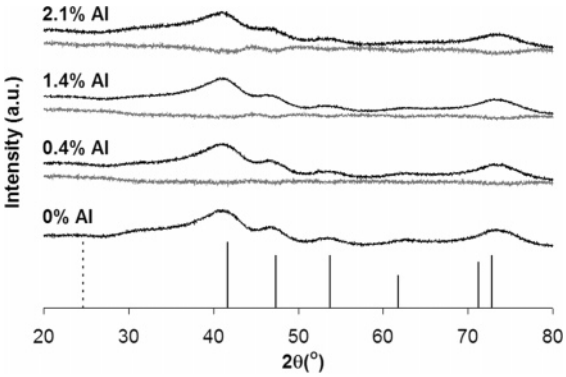

Figure 1. XRD patterns of the 0%, 0.4%, 1.4%, and 2.1% aluminum-substituted ferrihydrites. Diffraction patterns are shown in black. Difference plots, which are determined by subtracting the 0% Al pattern from each Al-substituted pattern, serve to highlight small shifts in peak positions and are shown in gray beneath each pattern. All patterns are consistent with the reference pattern for 6-line ferrihydrite, shown as solid lines (—). No evidence of goethite was observed in the patterns, and the reference peak for the strongest goethite reflection is shown as a dashed line (- - -).

TABLE 1: Aluminum Content (mol % Substitution) and Concentrations of Possible Contaminants (ppm) as Determined Using ICP-MS

synthesis	aluminum content (mol %)	sodium content (ppm)	arsenic content (ppm)
ferrihydrite, 0.48 M base	0.0	136	16
ferrihydrite w/5% Al, 0.48 M base	0.4	163	8
ferrihydrite w/20% Al, 0.48 M base	1.4	307	7
ferrihydrite w/30% Al, 0.60 M base	2.1	80	6

HPLC Method. Filtrates were analyzed using an Agilent HPLC equipped with a Zorbax C_{18} column. The mobile phase was a 65:35 mixture of acetate buffer and acetonitrile, and a flow rate of 0.75 mL/min and a 10 μL injection volume were used. Hydroquinone eluted at 2.3 min and benzoquinone at 3.4 min. The absorbance at 235 nm was monitored, and eight-point calibration curves, ranging from 5 to 1000 μM for hydroquinone and 0.5 to 100 μM for benzoquinone, were used to determine concentrations.

Results and Discussion

ICP-MS. The composition of each ferrihydrite sample was determined using ICP-MS (See Table 1). The amount of aluminum present in each of the samples was substantially lower than the percentage of aluminum in the original solutions. This is most likely the result of the relatively high solubility of aluminum, certainly as compared to ferric iron solubility, under the conditions of the ferrihydrite synthesis.[1] The concentrations of possible contaminants (e.g., Na and As) were also measured and found to be lower than parts per thousand.

XRD. Powder X-ray diffraction (XRD) patterns show that the materials prepared were consistent with the reference pattern for 6-line ferrihydrite (Figure 1). No evidence for the presence of other iron oxides was detected. In addition, no significant

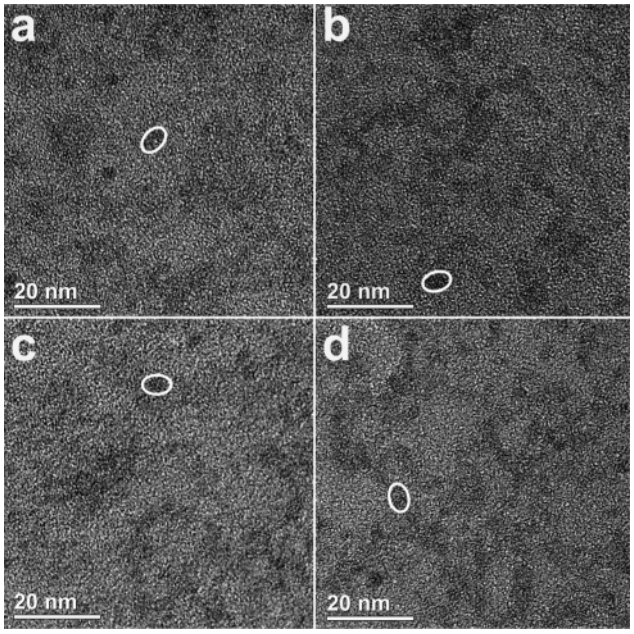

Figure 2. Representative TEM images of aluminum-substituted ferrihydrites: (a) 0% Al; (b) 0.4% Al (c) 1.4% Al; (d) 2.1% Al.

differences in the degree of crystallinity, which would be detected by changes in peak broadening and relative intensity, were apparent between samples. The most notable difference between the patterns was a slight peak shift toward higher angles in the aluminum-substituted samples, which is highlighted by the differential plots shown beneath each pattern for the Al-substituted ferrihydrites. This shift indicates a small but significant decrease in lattice spacings with aluminum substitution and supports the idea that aluminum was incorporated into the crystal structure of the particles. The peak shifts become more evident as the amount of aluminum substitution increases; this is consistent with previous work that showed a relationship between increasing aluminum content and a decrease in the atomic-plane spacing for several different iron oxide structures.[1]

TEM. A representative TEM image for each ferrihydrite sample is shown in Figure 2. Particle size measurements demonstrate that all samples were similar in particle size (4.4−4.5 by 3.5−3.7 nm) and aspect ratio (1.2). Average particle dimensions and calculated specific surface areas for each sample are shown in Table 2. The particle size distributions suggest that there is no statistical difference between the particle dimensions of the various samples, and the aggregation states of the samples appear similar. Thus, we believe that, at the low levels of Al substitution of this study, it can be assumed that the specific and accessible surface area is independent of aluminum substitution.

Kinetics. The expected half and overall reactions[9] between ferrihydrite and hydroquinone (QH_2) to produce benzoquinone (Q), aqueous Fe(II), and water can be expressed as

$$2Fe_5HO_8{\cdot}4H_2O(s) + 10e^- + 30H^+(aq) \rightarrow 10Fe^{2+}(aq) + 24H_2O(l)$$

$$5QH_2(aq) \rightarrow 5Q(aq) + 10e^- + 10H^+(aq)$$

$$2Fe_5HO_8{\cdot}4H_2O(s) + 5QH_2(aq) + 20H^+(aq) \rightarrow 10Fe^{2+}(aq) + 5Q(aq) + 24H_2O(l)$$

Rate constants were calculated using the measured rate of reaction, as determined using the method of initial rates,[18] and the literature values[9] for the orders with respect to hydroquinone and the particle surface (S) according to the rate law for the reaction

$$\frac{d[Q]}{dt} = k[QH_2]^m[S]^n$$

Here, k is the rate constant, and m and n are the empirical orders with respect to hydroquinone and the particle surface, respectively. It is assumed that these orders are independent of aluminum content, and this assumption was verified for the 1.4% aluminum-substituted sample (results not shown). In addition, the concentration of surface sites is assumed to be proportional to the surface area of the particles and, therefore, to the mass of the material used for a constant particle size. It should be noted that the proton concentration has been incorporated into the rate constant, as all reactions were performed at a constant pH of 3.75.

The rate of each reaction was determined by fitting the initial, linear portion of the data for the rate of formation of benzoquinone (Figure 3). Data points were included in the linear fit as long as their inclusion did not cause a deviation from linearity. This resulted in four to eight data points from each trial (8−16 points for each sample) being included in each fit. When making comparisons between samples, reaction rates were mass normalized, since the specific surface areas are assumed to be similar for the materials studied, as previously discussed. The formation of benzoquinone in particle-free blanks was also monitored, and in all cases, the spontaneous conversion of hydroquinone to benzoquinone was one or more orders of magnitude slower than reaction rates (results not shown).

The rate of hydroquinone oxidation clearly increases with aluminum content (Figure 3), and this increase was more pronounced at higher temperatures. Transition state theory[19] was employed in order to determine the nature of the enhancement

TABLE 2: Average Particle Dimensions and Specific Surface Areas for Aluminum-Doped Ferrihydrite Nanoparticles as Determined Using TEM[a]

sample	particle length (nm)	particle width (nm)	surface area (m^2/g)
ferrihydrite	4.6 ± 0.4	3.7 ± 0.3	374 ± 30
0.4% Al-subst ferrihydrite	4.5 ± 0.5	3.6 ± 0.5	375 ± 50
1.4% Al-subst ferrihydrite	4.6 ± 0.5	3.6 ± 0.4	373 ± 43
2.1% Al-subst ferrihydrite	4.5 ± 0.5	3.5 ± 0.5	385 ± 48

[a] The errors reported are standard errors.

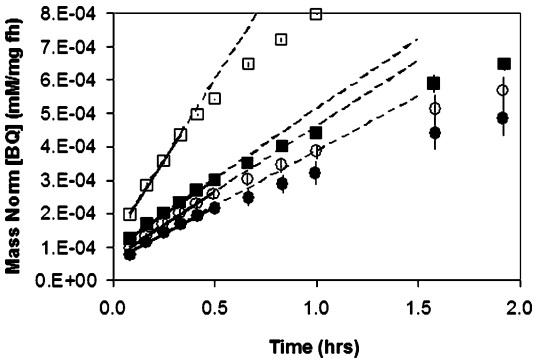

Figure 3. Mass-normalized concentration of benzoquinone as a function of time. Solid lines represent the linear regression and have been extended with a dashed line for clarity: (●) ferrihydrite (fh); (○) 0.4% Al-subst fh; (■) 1.4% Al-subst fh; (□) 2.1% Al-subst fh.

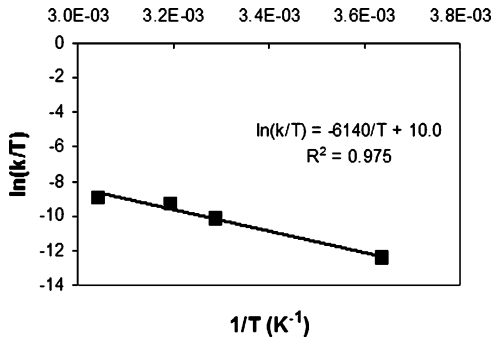

Figure 4. Application of the Eyring equation to temperature series for 1.4% Al-substituted ferrihydrite. The line shown is the linear fit of the data.

in reactivity. The natural log of the Eyring equation produces a linear relationship between ln(k/T) and $1/T$

$$\ln\frac{k}{T} = \ln\frac{k_B}{h} + \frac{\Delta S^{\ddagger}}{R} - \frac{\Delta H^{\ddagger}}{RT}$$

Here, k is the rate constant for the reaction, T is absolute temperature, k_B is Boltzmann's constant, h is Planck's constant, R is the gas constant, and $\Delta S^{\ddagger}$ and $\Delta H^{\ddagger}$ are activation entropy and enthalpy, respectively. The slope of the line obtained using this equation is proportional to the activation enthalpy, while the activation entropy can be extracted from the intercept (Figure 4). By performing each reaction at a series of four temperatures and using the empirical rate law to determine the rate constant at each temperature, activation entropy and enthalpy can be calculated. The reaction mechanisms, and thus empirical orders, are not expected to change within the temperature range studied. This assumption is based on kinetic studies of hydroquinone oxidation by ferrihydrite that indicated that although the system becomes more complicated at temperatures above 65 °C, there is no evidence to support a change in mechanism at temperatures lower than 60 °C.[20]

The results of these calculations demonstrate that there is an inverse relationship between the activation free energy ($\Delta G^{\ddagger}$) and the amount of aluminum present (see Figure 5a). As the amount of aluminum substitution increases, an increase in the activation entropy ($\Delta S^{\ddagger}$) (Figure 5b) and a decrease in the activation enthalpy ($\Delta H^{\ddagger}$) (Figure 5c) are observed. An increase in $\Delta S^{\ddagger}$ likely arises from the introduction of the aluminum cation, which serves to greater diversify the transition states available during the reaction. The positive value of $\Delta S^{\ddagger}$ indicates that the transition state is more disordered than the reactants, and the increase in magnitude suggests that the transition states for the particles containing aluminum are relatively more disordered than those of the pure ferrihydrite particles. This increase in activation entropy signifies that there is a greater probability that a collision between reactants will result in the formation of products. Therefore, the introduction of a small amount of aluminum, which will only slightly reduce the number of reactive sites, is expected to greatly influence reactivity. This trend is consistent with kinetic data presented by Gonzalez, Ballesteros, and Rueda that showed an increase in frequency factor with increasing aluminum content for substituted goethites.[11]

The decrease in $\Delta H^{\ddagger}$ with increasing aluminum content suggests that the aluminum substitution destabilizes the particle reactant. The substitution of an aluminum cation for an iron cation results in the contraction of the lattice parameter,[1] as supported by the XRD data. This mismatch of ionic radii would introduce strain into the crystal lattice, resulting in the destabilization of the bonds and allowing the ferrihydrite nanoparticle to more readily dissolve. The aluminum cation is therefore serving as a nonreactive species that destabilizes the reactive sites on the surface because of the slight differences in bond angles and lengths that would occur as a result of the different ionic radii. The resulting decrease in $\Delta H^{\ddagger}$ combines with the increase in $\Delta S^{\ddagger}$ to cause a decrease in $\Delta G^{\ddagger}$ as a function of aluminum substitution and enhance the reactivity of ferrihydrite particles with small amounts of aluminum substitution. This effect on reactivity is likely to also be applicable to other, less environmentally relevant, cation substitutions.

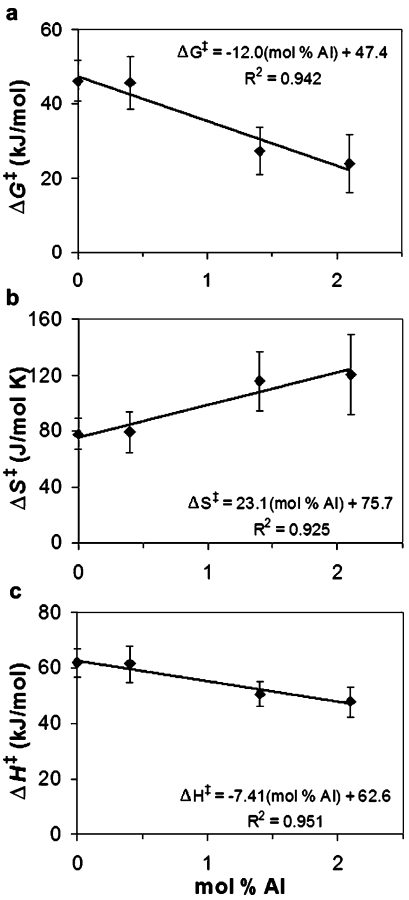

Figure 5. Plots of (a) activation free energy, (b) activation entropy, and (c) activation enthalpy as a functions of increasing aluminum substitution. Lines represent the linear regression. Error bars represent the standard deviation obtained from the duplicate experiments performed at four temperatures.

Conclusions

The results of this work show an increase in $\Delta S^{\ddagger}$, a decrease in $\Delta H^{\ddagger}$, a decrease in $\Delta G^{\ddagger}$, and, therefore, an overall increase in the reactivity of ferrihydrite particles with increasing aluminum substitution in the range of 0−2.1 mol %. These results are consistent with those of other iron oxides with small amounts of substitution (i.e., goethite[11]). The enhanced reactivity displayed by aluminum-bearing iron oxides may allow them to participate in the cycling of other species in the environment more efficiently than pure iron oxides. These results provide additional understanding of the solid-state materials present in groundwater and soil systems. It is expected that as aluminum content increases further, there will be a level at which the substitution eliminates a significant number of reactive iron sites, causing a decrease in the frequency factor and thus a reversal in the reactivity trend, as has been observed in the goethite

system.[11] Future work will focus on increasing the aluminum content in ferrihydrite samples without substantially changing size and morphology to determine whether there is a reversal in reactivity.

Acknowledgment. We thank 3M (fellowship to T.L.J.), the University of Minnesota, and the National Science Foundation (NSF-CAREER 0346385 and NSF-MRI EAR-0320641) for funding. We thank Rick Knurr for the ICP-MS analyses.

References and Notes

(1) Cornell, R. M.; Schwertmann, U. *The Iron Oxides: Structure, Properties, Reactions, Occurrences and* Uses, 2nd ed.; Wiley-VCH: Weinheim, 2003.

(2) Graham, R. C.; Weed, S. B.; Bowen, L. H.; Amarasiriwardena, D. D.; Buol, S. W. *Clays Clay Miner.* **1989**, *37*, 29.

(3) Casiot, C.; Lebrun, S.; Morin, G.; Bruneel, O.; Personne, J. C.; Elbaz-Poulichet, F. *Sci. Total Environ.* **2005**, *347*, 122.

(4) Jessen, S.; Larsen, F.; Koch, C. B.; Arvin, E. *Environ. Sci. Technol.* **2005**, *39*, 8045.

(5) Lovley, D. R. *Microbiol. Rev.* **1991**, *55*, 259.

(6) Schwertmann, U.; Friedl, J.; Stanjek, H.; Schulze, D. G. *Clay Miner.* **2000**, *35*, 613.

(7) Houben, G. J. *Appl. Geochem.* **2003**, *18*, 927.

(8) Jambor, J. L.; Dutrizac, J. E. *Chem. Rev.* **1998**, *98*, 2549.

(9) Anschutz, A. J.; Penn, R. L. *Geochem. Trans.* **2005**, *6*, 60.

(10) Shaw, J. N. *Commun. Soil Sci. Plant Anal.* **2001**, *32*, 49.

(11) Gonzalez, E.; Ballesteros, M. C.; Rueda, E. H. *Clays Clay Miner.* **2002**, *50*, 470.

(12) Kukkadapu, R. K.; Zachara, J. M.; Smith, S. C.; Fredrickson, J. K.; Liu, C. *Geochim. Cosmochim. Acta* **2001**, *65*, 2913.

(13) Stack, A. G.; Rosso, K. M.; Smith, D. M. A.; Eggleston, C. M. *J. Colloid Interface Sci.* **2004**, *274*, 442.

(14) Kung, K. H.; McBride, M. B. *Clays Clay Miner.* **1988**, *36*, 303.

(15) Scott, D. T.; McKnight, D. M.; Blunt-Harris, E. L.; Kolesar, S. E.; Lovley, D. R. *Environ. Sci. Technol.* **1998**, *32*, 2984.

(16) Newman, D. K.; Kolter, R. *Nature (London)* **2000**, *405*, 94.

(17) Burleson, D. J.; Penn, R. L. *Langmuir* **2005**, in press.

(18) Steinfeld, J. I.; Francisco, J. S.; Hase, W. L. *Chemical Kinetics and Dynamics*, 2nd ed.; Prentice Hall: London, 1999.

(19) Espenson, J. H. *Chemical Kinetics and Reaction Mechanisms*, 2nd ed.; McGraw-Hill: New York, 2002.

(20) Anschutz, A. unpublished result.